21

# Sensitivity analysis and stochastic modelling of the effective properties for reinforced elastomers

Marcin Kamiński*,** and Bernd Lauke**
*Technical University of Łódź, Al. Politechniki 6, 90-924 Łódź
Poland
**Leibniz Institute of Polymer Research Dresden, Hohe Strasse 6, 01069 Dresden
Germany

## 1. Introduction

Determination of the sensitivity gradients as well as probabilistic moments of composite materials and even micro-heterogeneous structures was a subject of many both theoretical and computational analyses reported in (Christensen, 1977; Fu at al., 2009; Kamiński, 2005; Kamiński, 2009). Usually it was assumed that there exists some Representative Volume Element, small in comparison to the entire structure and on the basis of some boundary problem solution on this RVE (like uniform extension for example) the elastic or even inelastic effective tensors were determined. Therefore, using some well established mathematical and numerical methods, sensitivity (via analytical, gradient or Monte-Carlo) or probabilistic (using simulations, spectral analyses or the perturbations) were possible having quite universal character in the sense that the effective tensors formulas are independent of the constituents design. Let us remind also that this cell problem was solved most frequently using rather expensive Finite Element Method based computations (even to determine the hysteretic multi-physics behavior) and did not allow full accounting for the reinforcing particles interactions or the other chemical processes between the components modeling. The challenges in the nanomechanics as one may recognize also below are slightly different – although one needs to predict the effective behavior of the solid reinforced with the nanoparticles, the formulas for effective properties may be addressed through experimental results calibration to the specific components. Such an experimental basis makes it possible to give analytical formulas even for the strain-dependent material models, which was rather impossible in the micromechanics before. Furthermore, it is possible now to account for the particle agglomeration phenomenon, where the dimensionless parameter describing this agglomeration size is directly included into the effective parameter model (Bhowmick, 2008; Heinrich et al., 2002a). Taking this development into consideration, there is a need to answer the question – how the particular models for those effective parameters (like shear modulus here) are sensitive to the design parameters included into the particular model. Moreover, taking into account manufacturing and experimental

statistics it is necessary to determine how this uncertainty (or even stochasticity) propagates and influences probabilistic characteristics of the effective parameters.
Therefore, the main now is to collect various models for the effective shear modulus describing the solids with nanoparticles, group them into some classes considering the similarities in the mathematical form of the physical assumptions. Next, sensitivity gradients of input parameters are determined and the probabilistic characteristics are considered by a randomization of those parameters and, finally, we study some of those theories in the presence of stochastic ageing under non-stationary stochastic processes. Mathematical basis for those studies is given by the stochastic generalized perturbation theory, where all random parameters and functions are expanded via Taylor series with random coefficients. A comparison of the same order quantities and classical integration known from the probability theory allows for a determination of the desired moments and coefficients with a priori assumed accuracy. Now up to fourth order central probabilistic moments as well as the coefficients of variation, asymmetry and concentration are computed – computational part is completed thanks to the usage of symbolic algebra system MAPLE. The main advantage of the perturbation method applied behind the Monte-Carlo simulation is that the preservation of a comparable accuracy is accompanied now by significantly smaller computational time and, further, parametric representation of the resulting moments. Let us mention that the sensitivity analysis is the inherent part of the perturbation approach – since first order partial derivatives are anyway necessary in the equations for the probabilistic moments (up to $10^{th}$ order derivatives are computed now). Finally, the stochastic ageing phenomenon was modeled, where the output probabilistic moments time fluctuations were obtained. The results obtained and the methods applied in the paper may be further used in optimization of the effective parameters for solids with nanoparticles as well as reliability (and/or durability) analysis for such materials or structures made of them.

## 2. Comparison of various available theories

As it is known from the homogenization method history, one of the dimensionless techniques leading to the description of the effective parameters is the following relation describing the shear modulus:

$$G^{(eff)} = f\, G_0\,, \tag{1}$$

where $G_0$ stands for the virgin, unreinforced material and $f$ means the coefficient of this parameter increase, related to the reinforcement portion applied into it. As it is known, the particular characterization of this coefficient strongly depends on the type of the reinforcement - long or short fibers or reinforcing particles, arrangement of this reinforcement – regular or chaotic, scale of the reinforcement related to the composite specimen (micro or nano, for instance) or, of course, the volumetric ratios of both constituents. It is not necessary to underline that the effective nonlinear behavior of many traditional and nano-composites, not available in the form of simple approximants, needs much more sophisticated techniques based usually on the computer analysis with the use of the Finite Element Method. Let us note also that the elastomers are some specific composite materials, where usually more than two components are analyzed – some interface layers are inserted also (Fukahori, 2004) between them (the so-called SH and GH layers), which

practically makes this specimen 4-component. Therefore, traditional engineering and material-independent theories for the effective properties seem to be no longer valid in this area (Christensen, 1977).

The development of effective shear modulus for the elastomers resulted in various models, which can be generally divided into (a) linear theories based on the volume fractions of the inclusions, (b) linear elastic fractal models as well as (c) stress-softening fractal models. The first group usually obeys the following, the most known approximations, where the coefficient *f* is modeled using

- Einstein-Smallwood equation

$$f = 1 + 2.5\varphi\,, \tag{2}$$

- Guth-Gold relation

$$f = 1 + 2.5\varphi + 14.1\varphi^2\,, \tag{3}$$

- Pade approximation

$$f = 1 + 2.5\varphi + 5.0\varphi^2 + \ldots \cong 1 + \frac{2.5\varphi}{1 - 2\varphi}\,, \tag{4}$$

where φ is the inclusions volume fraction; eqn (2) is introduced under the assumptions on perfect rigidity of the reinforcing particles and the elastomeric matrix incompressibility. The effectiveness of those approximations is presented in Fig. 1, where the parameter φ belongs to the interval [0.0,0.4] resulting in the range of the coefficient f varying from 1 (effective parameter means simply virgin material modulus) up to about 6 at the end of φ variability interval. As it can be expected, the Einstein-Smallwood approximation gives always the lower bound, whereas the upper bound is given by Guth-Gold approach for $0 \le \varphi \le 0.325$ and by Padè approximation for $\varphi \ge 0.325$. Taking into account the denominator of eqn (4) one must notice that the singularity is observed for φ=0.5 and higher volume ratios returns the negative results, which are completely wrong, so that this value is the upper bound of this model availability. The other observation of rather general character is that now the increase of shear modulus is measured not in the range of single percents with respect to the matrix shear modulus value (like the composites with micro-inclusions) but is counted in hundreds of percents, which coincides, for example with the results obtained for the effective viscosities of the fluids with solid nano-particles.

The second class of the homogenized characteristics is proposed for elastomers taking into account the fractal character of the reinforcing particles chains and can be proposed as

$$f \cong 1 + \begin{cases} \Xi^{-\frac{1}{4}}\,\varphi, & \varphi < \varphi_c \\ \Xi^{-\frac{5}{4}}\,\varphi^4, & \varphi > \varphi_c \end{cases} \tag{5}$$

where

$$\Xi = \frac{\xi}{b} \tag{6}$$

is also dimensionless parameter relating cluster size $\xi$ to the size of the primary particle of carbon black constituting the reinforcing aggregate diameter ($b$). The condition that $\varphi < \varphi_c$ means that no aggregate overlap (smaller concentrations coefficients); otherwise the second approximation in eqn (5) is valid. The introduction of parameter $\Xi$ enables to analyze the whole spectra of elastomers without precise definition of their aggregates dimensions in *nm*. The response surface of the coefficient *f* with respect to two input quantities $\varphi \in [0.0,0.4]$ and $\Xi \in [1.0,10.0]$ is given below – the upper surface is for the non-overlapping situation, while the lower one – for the aggregates overlap. Both criteria return the same, intuitionally clear, result that the larger values of both parameters the larger final coefficient *f*, however now, under the fractal concept, its value is essentially reduced and is once more counted in percents to the original unreinforced matrix value. Observing the boundary curves for $\varphi_{max}$ it is apparent that this increase for overlapping and not overlapped cases has quite different character.

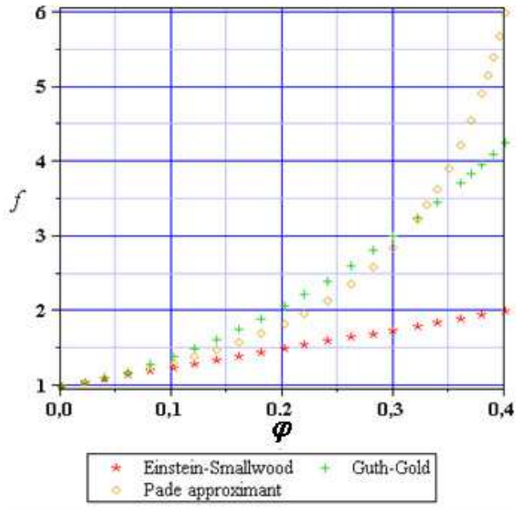


Fig. 1. A comparison of various volumetric approximations for the coefficient f

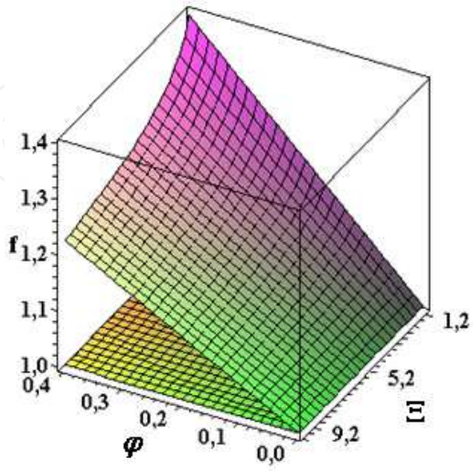


Fig. 2. Coefficient f for the rubbers with the carbon black aggregates by DLA clusters

The model presented above is, as one can compare, the special case of more general approach, where it is assumed

$$f \cong 1 + \begin{cases} \Xi^{2\frac{d_f}{D}-2d_f} \varphi, & \varphi < \varphi_c \\ \Xi^{2\frac{d_f}{D}-d_f} \varphi^{\frac{2}{3-d_f}}, & \varphi > \varphi_c \end{cases} \tag{7}$$

$d_f$ means the mass fractal dimension and $D$ is the spectral dimension as a measure of the aggregate connectivity (it is enough to put $d_f$=2.5 and $D$=4/3 to obtain eqn (5)). This equation has no parameter visualization according to the larger number of the independent variables.

Finally, the homogenization rules under stress-softening were considered- with Mullins effect (Dorfmann et al., 2004), where for carbon black and silica reinforcements the overlapped configuration $\varphi > \varphi_c$ was noticed. Additionally, the cluster size ξ was considered as the deformation-dependent quantity $\xi = \xi(E)$ with $E$ being some scalar deformation variable related explicitly to the first strain tensor invariant, however, some theories of deformation independent cluster sizes are also available. Those theories are closer to the realistic situations because the function $\xi = \xi(E)$ is recovered empirically and it results in the following formulas describing the coefficient $f$ varying also together with the strain level changes:

- the exponential cluster breakdown

$$f(E) = X_\infty + (X_0 - X_\infty)\exp(-\alpha E) \tag{8}$$

and

- the power-law cluster breakdown

$$f(E) = X_\infty + (X_0 - X_\infty)(1+E)^{-y}. \tag{9}$$

The following notation is employed here

$$X_\infty = 1 + C\left(\frac{\xi_0}{b}\right)^{d_w - d_f} \varphi^{\frac{2}{3-d_f}}, \qquad X_0 = 1 + C\varphi^{\frac{2}{3-d_f}}, \tag{10,11}$$

where $C \in \Re$ and $d_w$ is the fractal dimension representing the displacement of the particle from its original position. Because $\xi_0$ stands for the initial value of the parameter ξ one can rewrite eqn (10) as

$$X_0 = 1 + C\Xi^{d_w - d_f} \varphi^{\frac{2}{3-d_f}}. \tag{12}$$

Below one can find numerical illustration of those parameters variability for some experimentally driven combinations of the input parameters for the specific elastomers.

As one may expect, larger volumetric fractions of the reinforcement lead to larger values of the coefficient f; the smaller the values of the strain measure E the more apparent differences

between the values f are computed for various combinations of materials and their volumetric ratios. Comparison of Figs. 3 and 4 shows that independently from the model (exponential or power-law) the smallest values of the parameter f are computed for 40% silica reinforcement, and then in turn – for 40% carbon black, 60% silica and 60% carbon black. So that it can be concluded that, in the context of the coefficient f, the carbon black reinforcement results in larger reinforcement of the elastomer since $G^{(eff)}$ is higher than for the reinforcement by silica for the same volumetric amount of those particles. Comparing the results for all models presented in Figs. 1-4 one can generally notice that the power-law cluster breakdown theory returns the largest values of the studied coefficient f for small values of the stretch of the elastomer analyzed.

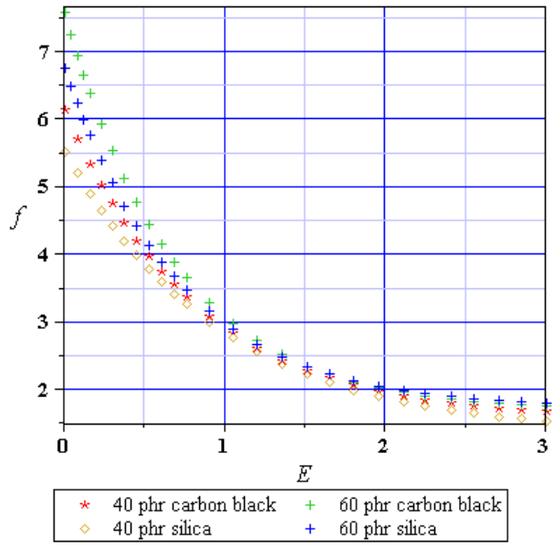


Fig. 3. The curve f=f(E) for the exponential cluster breakdown

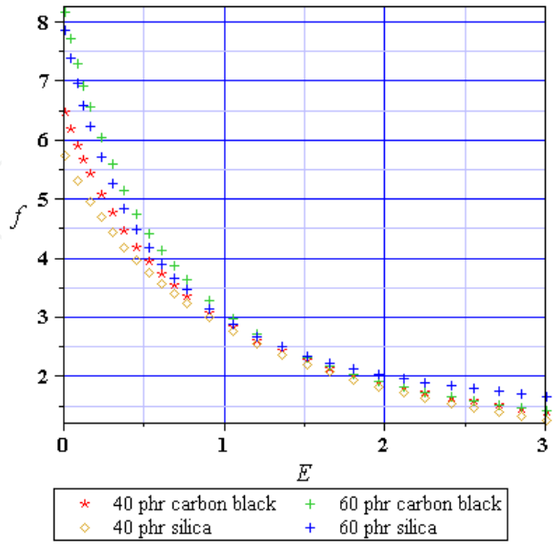


Fig. 4. The curve f=f(E) for the power-law cluster breakdown

## 3. Design sensitivity analysis

As it is known from the sensitivity and optimization theory, one of the milestones in the optimal design of the elastomers would be numerical (or analytical when available) determination of the sensitivity coefficients for the effective modulus as far as the homogenization theory is employed in the design procedure. Then, by simple partial differentiation of initial eqn (1) with respect to some elastomers design parameter $h$ one obtains

$$\frac{\partial G^{(eff)}}{\partial h} = \frac{\partial f}{\partial h} G_0 + f \frac{\partial G_0}{\partial h} . \tag{13}$$

Considering the engineering aspects of this equation, the second component of the R.H.S. may be neglected because the design parameters are connected in no way with the unreinforced material, so that the only issue is how to determine the partial derivatives of the coefficient $f$ with respect to some design variables like the volumetric ratio of the reinforcement, the cluster size, the exponents and powers as well as the strain rate in stress-dependent models. Further usage of those sensitivities consists in determination of the response functional, like strain energy of the hyperelastic effective medium for the representative stress state on the elastomer specimen, a differentiation of this functional w.r.t. design parameter and, finally, determination of the additional optimal solution.
First, we investigate the sensitivity coefficients as the first partial derivatives of the coefficient f with respect to the reinforcement volumetric ratio, accordingly to the analysis performed at the beginning of Sec. 2. As it could be expected (see Fig. 5), the Einstein-Smallwood returns always positive constant value, which is interpreted obviously that the higher coefficient $\varphi$, the larger value of the parameter $f$. The remaining gradients are also always positive, whereas the upper bounds gives the Guth-Gold model in the interval $\varphi \in [0.0,0.25]$, for larger volumetric ratios of the reinforcement the Padè approximation exhibit almost uncontrolled growth.

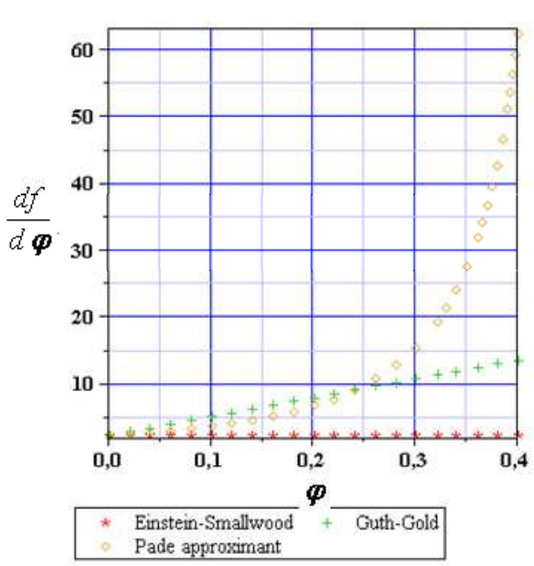


Fig. 5. Sensitivity coefficients for the volumetric coefficient f

The next results computed deal with the sensitivity coefficients of the coefficient *f* for the theory including the fractal character of the reinforcement for the non-overlapped and overlapped configurations of the elastomer, however now there are two design variables – the volumetric ratio φ as well as the parameter Ξ; the results are given in Figs. 6-7 accordingly, where larger absolute values are obtained in both cases for the elastomer with no overlapping effect.

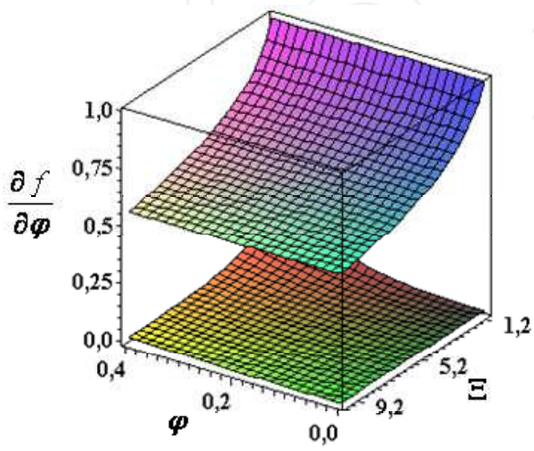


Fig. 6. Sensitivity for rubbers with carbon black aggregates by DLA clusters to volumetric ratio of the reinforcement

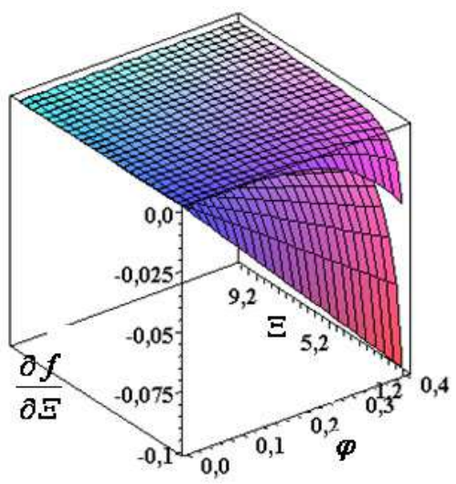


Fig. 7. Sensitivity for rubbers with carbon black aggregates by DLA clusters to Ξ

As it is quite clear from those surfaces variability, when the model with overlapping is considered, the resulting sensitivity gradients are dependent in a comparable way on both parameters φ and Ξ. However, the model with the overlap effect exhibits significant changes to the parameter Ξ, while almost no – with respect to the variable φ. Further, one may find easily that the lower value of Ξ (dimensionless cluster size), the higher are the gradients with respect to φ. Physical interpretation of this result is that the elastomers with the reinforcing particles more independent from each other are more sensitive to this

reinforcement volumetric ratios than the elastomers with larger clusters. Both models return here positive values, so that increasing of those parameters return an increase of the studied gradient value. Fig. 7 contains analogous results for the gradients computed with respect to the cluster size Ξ and now, contrary to the previous results, all combinations of input parameters return negative gradients. This gradient is almost linearly dependent on the parameter φ for the case without overlapping and highly nonlinear w.r.t. Ξ, whereas the overlap effect results in similar dependence of these gradients on both parameters. Quite analogously to the previous figure, the smaller value of the parameter Ξ, the larger output gradient value and opposite interrelation of this gradient to parameter φ.

Finally, we study the sensitivity coefficients for the exponential and power-law cluster breakdown with respect to the scalar deformation variable E (the results are presented in Figs. 8 and 9). Contrary to the previous sensitivity gradients, all the results are negative as one could predict from Figs. 3 and 4. Significantly larger absolute values are obtained for the exponential cluster breakdown here but, independently from the model, the highest sensitivity is noticed for $E \cong 0$ and then it systematically increases (its absolute values) to almost 0 for $E \cong 3$ and the differences between the elastomers with various reinforcement ratios monotonously vanish. The interrelations between different elastomers sensitivities depends however on the model and the power-law the largest absolute values are obtained for 60% carbon black; then in turn we have 60% silica, 40% carbon black and 40% silica. So, the carbon black reinforcement leads to larger sensitivity of the elastomer for the strain ratio E in the power-law cluster breakdown concept. The exponential model shows somewhat different tendency – 60% carbon black and 60% silica return almost the same gradients values where those first are little larger for intermediate values of E. The sensitivity of the carbon black elastomer apparently prevails, however for smaller amount of the reinforcement.

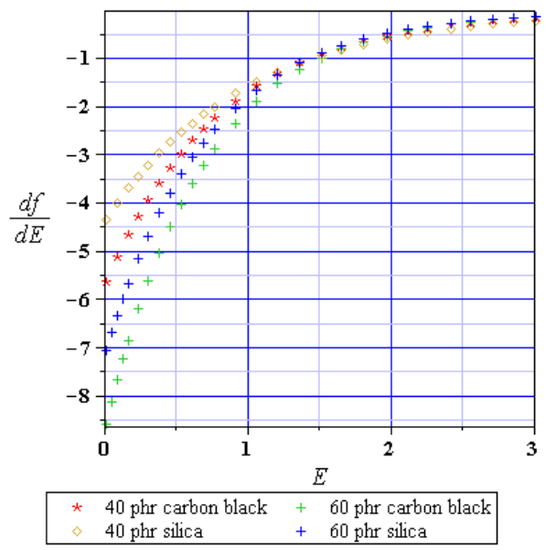


Fig. 8. Sensitivity coefficients for the exponential cluster breakdown via the scalar variable E

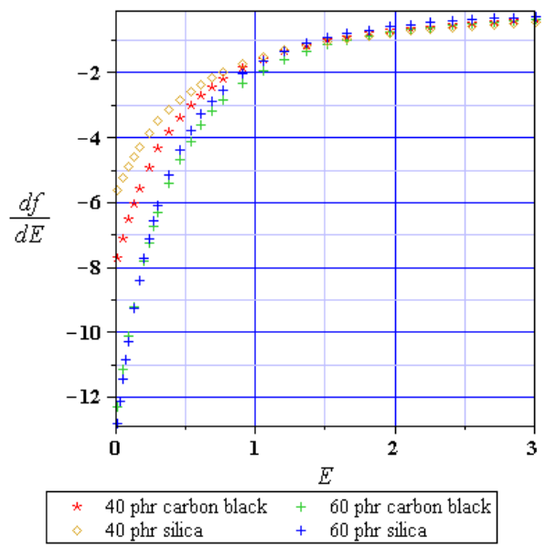


Fig. 9. Sensitivity coefficients for the power-law cluster breakdown to the scalar variable E

## 4. Effective behaviour for the elastomers with random parameters

The next step towards a more realistic description of the effective modulus for the elastomers reinforced with some fillers is probabilistic analysis, where some composite parameters or even their larger group is considered as the random variable or the vector of random variables. As is it known, there exists a variety of different mathematical approaches to analyze such a problem like determination of the probabilistic moments for $G^{(eff)}(\omega)$. One may use the algebraic transforms following basic probability theory definitions, Monte-Carlo simulation approaches, some spectral methods as well as some of the perturbation methods. Because the statistical description for $G_0(\omega)$ comes from the experiments we will focus here on determination of the random characteristics for $f(\omega)$ only. Because of some algebraic complexity of especially eqns (7-12) the stochastic perturbation technique based on the Taylor series expansion will be employed. To provide this formulation the random variable of the problem is denoted by $b(\omega)$ and the probability density of it as $g(b)$. The expected value of this variable is expressed by

$$E[b] = \int_{-\infty}^{+\infty} b\, g(b) db\,, \tag{14}$$

while the $m$th order moment as

$$\mu_m(b) = \int_{-\infty}^{+\infty} (b - E[b])^m g(b) db\,. \tag{15}$$

The coefficient of variation, asymmetry, flatness and kurtosis are introduced in the form

$$\alpha(b)=\frac{\sqrt{\mu_2(b)}}{E[b]}=\frac{\sqrt{Var(b)}}{E[b]}=\frac{\sigma(b)}{E[b]},\quad \beta(b)=\frac{\mu_3(b)}{\sigma^3(b)},\quad \gamma(b)=\frac{\mu_4(b)}{\sigma^4(b)},\quad \kappa(b)=\gamma(b)-3. \tag{16}$$

According to the main philosophy of this method, all functions in the basic deterministic problem (heat conductivity, heat capacity, temperature and its gradient as well as the material density) are expressed similarly to the following finite expansion of a random function *f*:

$$f(b)=f^0(b)+\varepsilon f^{,b}(b)\Delta b+\ldots+\tfrac{1}{n!}\varepsilon^n\frac{\partial^n f(b)}{\partial b^n}\Delta b^n, \tag{17}$$

where ε is a given small perturbation (taken usually as equal to 1), $\varepsilon\Delta b$ denotes the first order variation of $b$ from its expected value

$$\varepsilon\Delta b=\delta b=\varepsilon(b-b^0), \tag{18}$$

while the *n*th order variation is given as follows:

$$\varepsilon^n\Delta b^n=(\delta b)^n=\varepsilon^n(b-b^0)^n. \tag{19}$$

Using this expansion, the expected values are exactly given by

$$\begin{aligned}E[f]=f^0(b^0)+\tfrac{1}{2}\varepsilon^2\frac{\partial^2(f)}{\partial b^2}\mu_2(b)+\tfrac{1}{4!}\varepsilon^4\frac{\partial^4(f)}{\partial b^4}\mu_4(b)+\tfrac{1}{6!}\varepsilon^6\frac{\partial^6(f)}{\partial b^6}\mu_6(b)\\ +\ldots+\tfrac{1}{(2m)!}\varepsilon^{2m}\frac{\partial^{2m}(f)}{\partial b^{2m}}\mu_{2m}(b)\end{aligned} \tag{20}$$

for any natural m with $\mu_{2m}$ being the ordinary probabilistic moment of $2m^{th}$ order. Usually, according to some previous convergence studies, we may limit this expansion-type approximation to the $10^{th}$ order. Quite similar considerations lead to the expressions for higher moments, like the variance, for instance

$$\begin{aligned}Var(f)=\int_{-\infty}^{+\infty}(f^0+\varepsilon\Delta bf^{,b}+\tfrac{1}{2}\varepsilon^2(\Delta b)^2f^{,bb}+\tfrac{1}{3!}\varepsilon^3(\Delta b)^3f^{,bbb}\\ +\tfrac{1}{4!}\varepsilon^4(\Delta b)^4f^{,bbbb}+\tfrac{1}{5!}\varepsilon^5(\Delta b)^5f^{,bbbbb}-E[f])^2p(b)db=\\ =\varepsilon^2\mu_2(b)f^{,b}f^{,b}+\varepsilon^4\mu_4(b)(\tfrac{1}{4}f^{,bb}f^{,bb}+\tfrac{2}{3!}f^{,b}f^{,bbb})\\ +\varepsilon^6\mu_6(b)((\tfrac{1}{3!})^2f^{,bbb}f^{,bbb}+\tfrac{1}{4!}f^{,bbbb}f^{,bb}+\tfrac{2}{5!}f^{,bbbbb}f^{,b})\end{aligned} \tag{21}$$

The third probabilistic moment may be recovered from this scheme as

$$\mu_3(f) = \int_{-\infty}^{+\infty} (f - E[f])^3 p(b) db = \int_{-\infty}^{+\infty} (f^0 + \varepsilon f^{,b} \Delta b + \tfrac{1}{2}\varepsilon^2 f^{,bb} \Delta b \Delta b + \ldots - E[f])^3 p(b) db \cong \tfrac{3}{2}\varepsilon^4 \mu_4(b)(f^{,b})^2 f^{,bb} + \tfrac{1}{8}\varepsilon^6 \mu_6(b)(f^{,bb})^3 \quad (22)$$

using the lowest order approximation; the fourth probabilistic moment computation proceeds from the following formula:

$$\mu_4(f) = \int_{-\infty}^{+\infty} (f - E[f])^4 p(b) db = \int_{-\infty}^{+\infty} (\varepsilon f^{,b} \Delta b + \tfrac{1}{2}\varepsilon^2 f^{,bb} \Delta b \Delta b + \ldots)^4 p(b) db \cong \varepsilon^4 \mu_4(b)(f^{,b})^4 + \tfrac{3}{2}\varepsilon^6 \mu_6(b)(f^{,b} f^{,bb})^2 + \tfrac{1}{16}\varepsilon^8 \mu_8(b)(f^{,b})^3 (f^{,bb})^4 \quad (23)$$

For the higher order moments we need to compute the higher order perturbations which need to be included into all formulas, so that the complexity of the computational model grows non-proportionally together with the precision and the size of the output information needed. This method may be applied as well to determine $G^{(eff)}(\omega)$ - one may apply the Taylor expansion to both components of the R.H.S. of eqn (1), differentiate it symbolically at least up to the given *n*th order (similarly to eqn (13) w.r.t. variable *h*) like below

$$\frac{\partial^n G^{(eff)}}{\partial b^n} = \sum_{k=0}^{n} \binom{n}{k} \frac{\partial^k f}{\partial b^k} \frac{\partial^{n-k} G_0}{\partial b^{n-k}} \quad (24)$$

and include those derivatives into the probabilistic moment equations shown above.

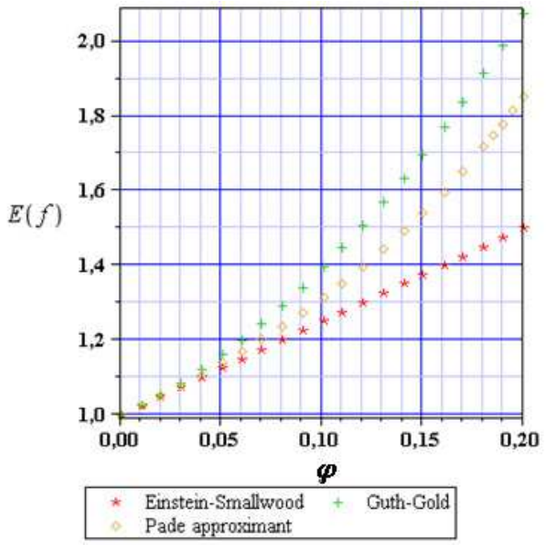


Fig. 10. The expected value of the volumetric coefficient f

The set of equations (20-23) with definitions given by (16) is implemented into the computer algebra system MAPLE, v. 11, as before, to determine the basic probabilistic characteristics for the function $f(\omega)$. The results of numerical analysis are presented in Figs. 10-25, where expected value of the input random variables are marked on the horizontal axes, its standard deviation corresponds to 15% of this expectation, while the output probabilistic moments of the parameter f are given on the vertical axes; the different theories for those coefficient calculations are compared analogously as in the previous sections. The Gaussian input random variables with given first two probabilistic moments are considered in all those computational illustrations

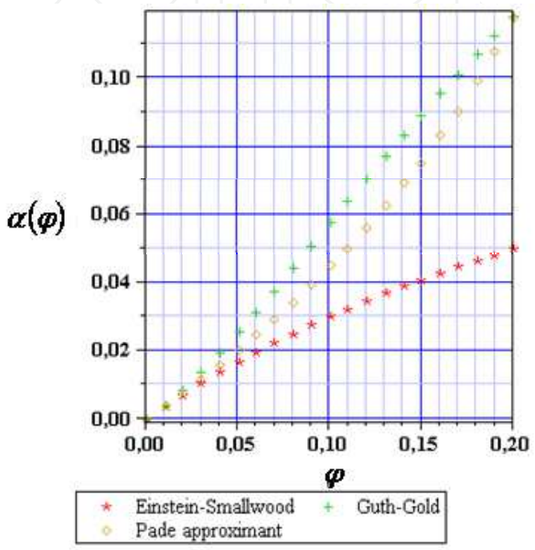


Fig. 11. The coefficient of variation of the volumetric coefficient f

Probabilistic moments and coefficients of up to 4th order of the simple volumetric approximations are given in Figs. 10-13 – there are in turn expected values, standard deviations, asymmetry and kurtosis. All the resulting functions increase here together with an increase of the reinforcement volumetric ratio φ. For the first two order characteristics the largest value is returned by the Guth-Gold model and the smallest - in the case of the Einstein-Smallwood approximation. Let us note also that the random dispersion of the output coefficient *f* is not constant and almost linearly dependent in all the models analyzed on the expected value of φ and is never larger here than the input value α(φ)=0.15. Third and fourth order characteristics demonstrate the maximum for the Guth-Gold theory for φ varying from 0 to the certain critical value, while for higher values the characteristics computed for the Pade approximants prevail significantly. All those characteristics are equal to 0 for the Einstein-Smallwood model because of a linear transform of the parameter φ in this model and it preserves exactly the character of the probability density function in a transform between the input φ and the output *f*. For the two remaining theories (with β>0) larger area of the probability density function remains above the expected value of *f*, while the concentration around this value if higher than for the Gaussian variables.

Now the basic probabilistic characteristics are compared for the homogenization model accounting for the clusters aggregation in the elastomers; the input coefficient φ is the input

Gaussian random parameter here also. Decisively larger values are obtained for the configuration without overlapping effect and all the characteristics are once more positive. In the case of expected values and standard deviations the influence of the coefficient φ on those quantities significantly prevail and has a clear linear character. A nonlinear variability with respect to Ξ is noticed for upper bound on the values of φ and has quite similar character in both Figs. 14 and 15. The maximum value of the coefficient of variation is about 0.02, which is around seven times smaller than the input coefficient, so that the random dispersion significantly decreases in this model.

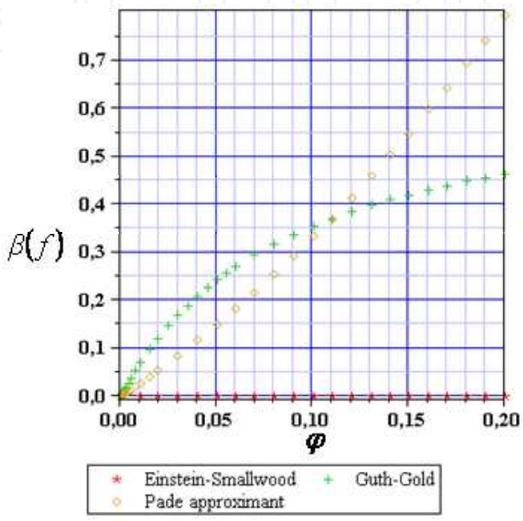


Fig. 12. The coefficients of asymmetry of the volumetric coefficient f

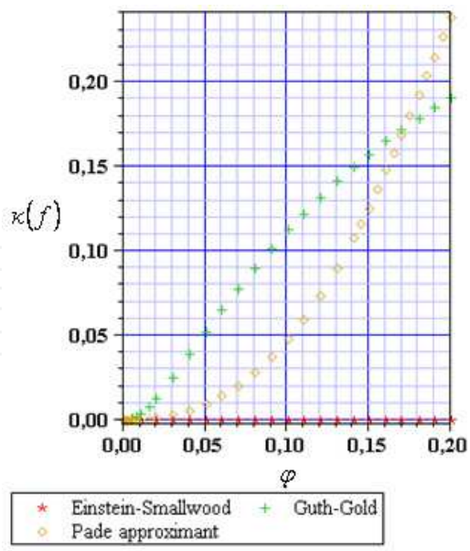


Fig. 13. The kurtosis of the volumetric coefficient f

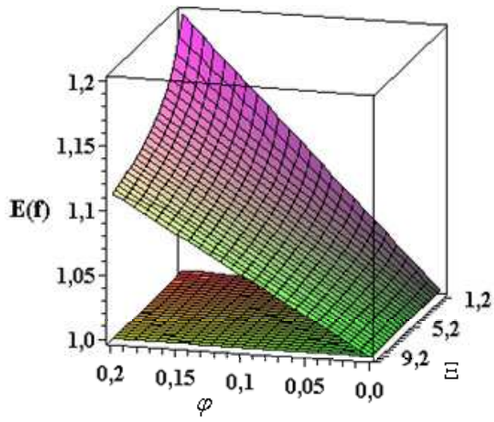


Fig. 14. The expected values of the coefficient *f* including aggregation

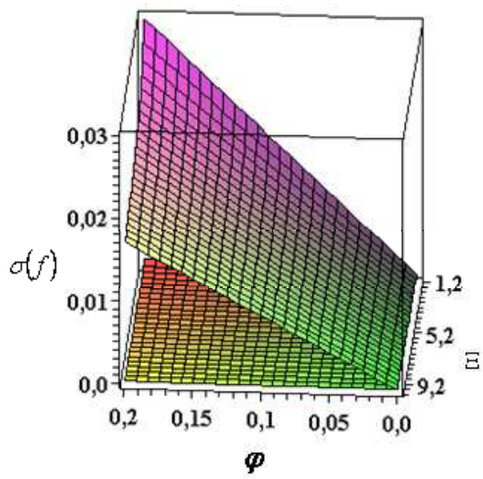


Fig. 15. The standard deviations of the coefficient *f* including aggregation

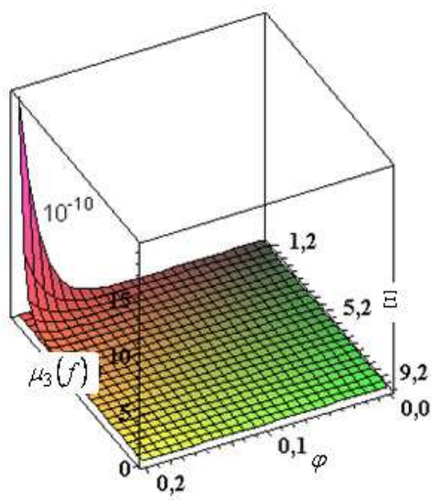


Fig. 16. Third central probabilistic moments of the coefficient *f* including aggregation

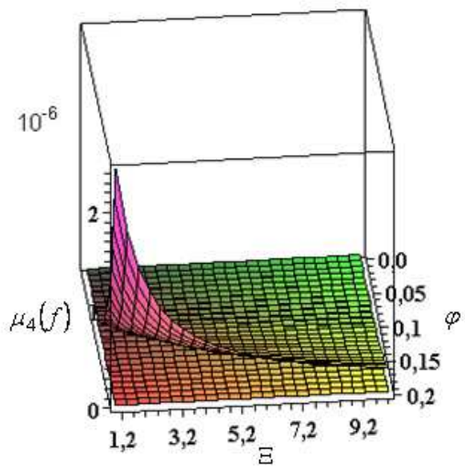


Fig. 17. Fourth central probabilistic moments of the coefficient *f* including aggregation

Third central probabilistic moments increase rapidly from almost 0 only for the smallest values of Ξ and largest values of φ – it results in β=0 for the overlapping aggregates and β=1.5 for the aggregates with no overlap. Fourth moments variations are more apparent for larger values of φ and the entire spectrum of the parameter Ξ. The resulting kurtosis equal 0 and almost 2 – without and with this overlap, respectively. It is seen that the larger values of φ and the smaller Ξ, the larger 3rd and 4th probabilistic moments. So that, analogously to the previous theories, larger part of the resulting PDF is above the median and its concentration is higher than that typical for the Gaussian distribution (for the model without aggregates overlapped). The distribution of the random parameter *f* is almost the same like for the Gaussian input (except the coefficient of variation).

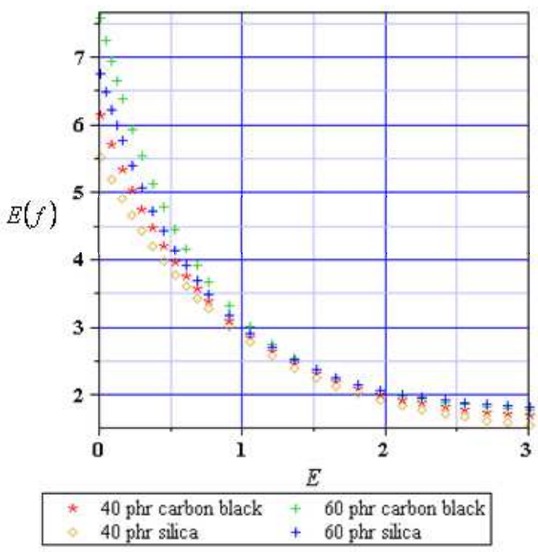


Fig. 18. The expected values for the exponential cluster breakdown to the scalar variable E

The probabilistic coefficients for the exponential (Figs. 18-21) and for the power-law (Figs. 22-25) cluster breakdowns are contrasted next; now the overall strain measure $E$ is the Gaussian input variable. As one may predict from the deterministic result, all the expected values decrease together with an increase of the $E$ expectation. The coefficient of variation α(f) (see Fig. 19) behave in a very interesting way – all they increase monotonously from 0 (for $E \cong 0$) to some maximum value (around a half of the considered strains scale) and next, they start to monotonously decrease; maximum dispersion is obtained for 60% of the carbon black here.

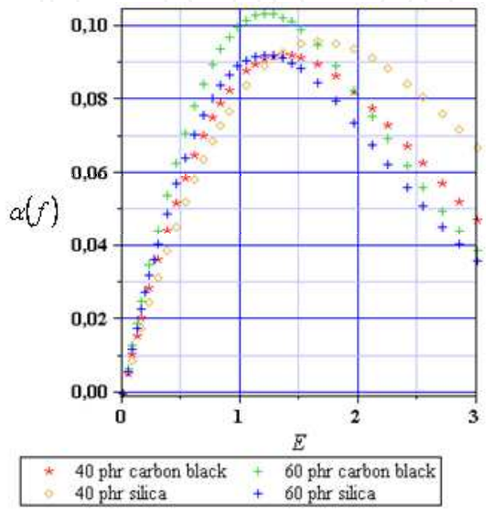


Fig. 19. Coefficients of variation for exponential cluster breakdown to the scalar variable E

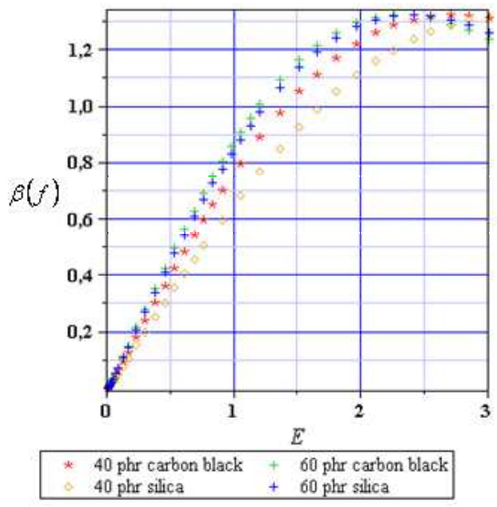


Fig. 20. Asymmetry coefficient for the exponential cluster breakdown to the scalar variable E

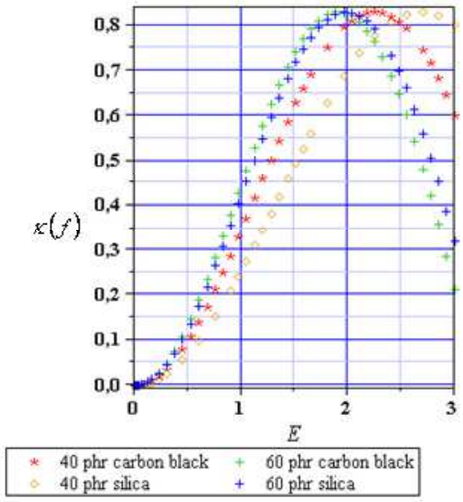


Fig. 21. The kurtosis for the exponential cluster breakdown to the scalar variable E

The asymmetry coefficient $\beta(f)$ and the kurtosis $\kappa(f)$ also behave similarly to $\alpha(f)$, where the additional maxima appear for larger and smaller values of the strain measure $E$; the coefficient $\beta(f)$ remains positive for all values of the parameter $E$. Within smaller $E$ values range we notice that larger values of both coefficients are observed for the carbon black and they increase also together with an increase of the reinforcement volumetric ratio. Similarly as before, the PDFs concentration is higher than that for the Gaussian distribution and a right part of resulting distributions prevail. The expected values for the power-law cluster breakdown are shown in Fig. 22; they decrease together with the expectation of the strain measure $E$ and the larger the reinforcement volume is, the larger is the expectation $E[f]$. The coefficients of variation are less predictable here (Fig. 23) – they monotonously increase for 40% of both reinforcing particles, whereas for 60% silica and carbon black they monotonously increase until some maximum and afterwards they both start to decrease; the particular values are close to those presented in Fig. 19.

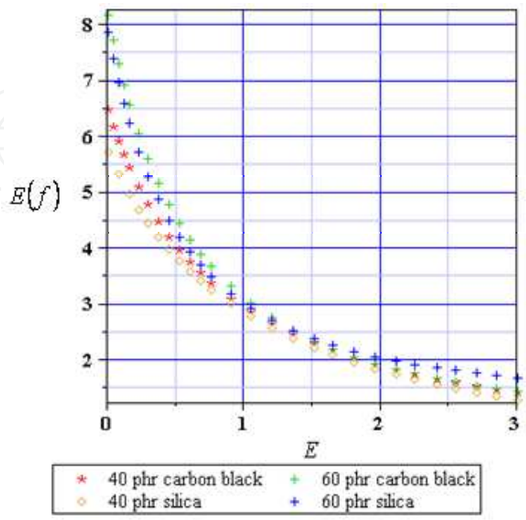


Fig. 22. The expected values for the power-law cluster breakdown to the scalar variable E

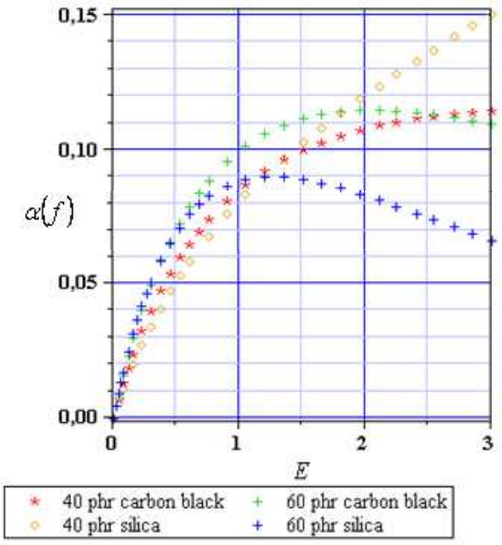


Fig. 23. Coefficients of variation for power-law cluster breakdown to the scalar variable E

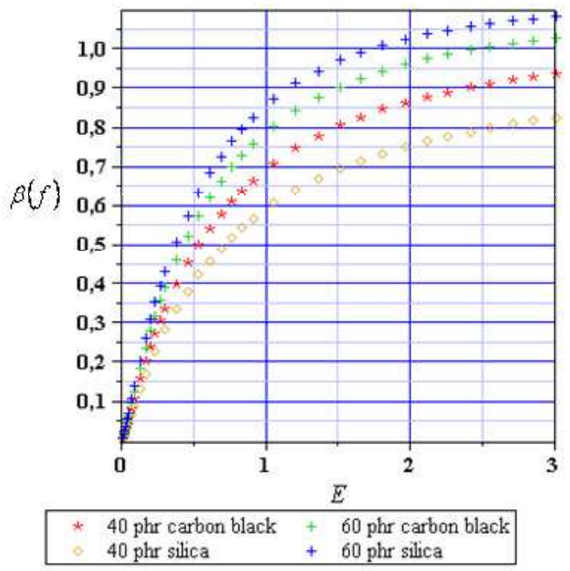


Fig. 24. Asymmetry coefficient for the power-law cluster breakdown to the scalar variable E

The coefficients of asymmetry and kurtosis do not increase as those in Figs. 20-21 – they simply monotonously increase from 0 value typical for E=0 to their maxima for E=3 (the only exception in this rule is kurtosis of the elastomer with 60% of the silica particles). Both coefficients have larger values for the carbon black than for silica and they increase together with the additional reinforcement volumetric ratio increase. Although coefficients of asymmetry exhibit the values quite close to those obtained for the exponential breakdown approach, the kurtosis is approximately two times smaller than before (Fig. 25 vs. Fig. 21).

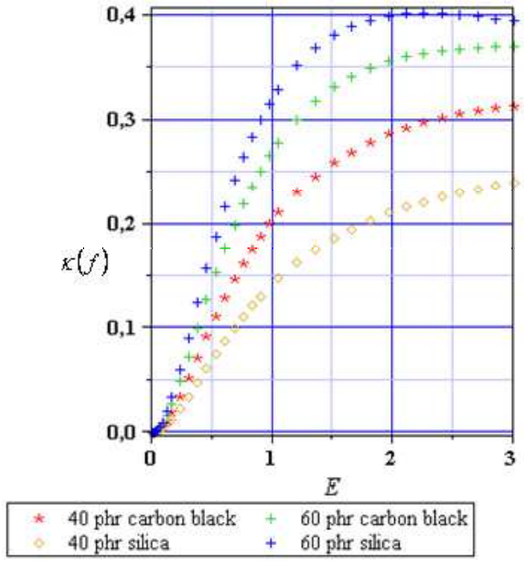


Fig. 25. The kurtosis for the power-law cluster breakdown to the scalar variable E

## 5. Homogenized parameters for elastomers subjected to the stochastic aging

The engineering practice in many cases leads to the conclusion that the initial values of mechanical parameters decrease stochastically together with the time being. As far as some periodic measurements are available one can approximate in some way those stochastic process moments, however a posteriori analysis is not convenient considering the reliability of designed structures and materials. This stochasticity does not need result from the cyclic fatigue loading (Heinrich et al., 2002b), but may reflect some unpredictable structural accidents, aggressive environmental influences etc. This problem may be also considered in the context of the homogenization method, where the additional formula for effective parameters may include some stochastic processes. Considering above one may suppose for instance the scalar strain variable $E$ as such a process, i.e.

$$E(\omega,t) = E^0(\omega) + \dot{E}(\omega)\, t \tag{25}$$

where superscript 0 denotes here the initial random distribution of the given parameter and dotted quantities stand for the random variations of those parameters (measured in years). From the stochastic point of view it is somewhat similar to the Langevin equation approach (Mark, 2007), where Gaussian fluctuating white noise was applied. It is further assumed that all aforementioned random variables in eqns (25,26) are Gaussian and their first two moments are given; the goal would be to find the basic moments of the process $f(\omega,t)$ to be included in some stochastic counterpart of eqn (1). The plus in eqn (25) suggests that the strain measure with some uncertainty should increase with time (Mark, 2007) according to some unpredictable deformations; introduction of higher order polynomium is also possible here and does not lead to significant computational difficulty. A determination of the first two moments of the process given by eqn (25) leads to the formulas

$$E[E(\omega,t)] = E[E^0(\omega)] + E[\dot{E}(\omega)]\,t \tag{26}$$

and

$$Var(E(\omega,t)) = Var(E^0(\omega,t)) + Var(\dot{E}(\omega,t))\,t^2 . \tag{27}$$

Now four input parameters are effectively needed to provide the analysis for stochastic ageing of any of the models presented above; the additional computational analysis was performed with respect to the exponential and power-law cluster breakdown models below. This part of computational experiments started from the determination of the expected values (Fig. 26), coefficients of variation (Fig. 27), the asymmetry coefficients (Fig. 28) and the kurtosis (Fig. 29) time fluctuations in the power-law model. For this purpose the following input data are adoped: $E[E_0] = 3$, $E[\dot{E}] = 0.03\ year^{-1}$, $Var(E_0) = (0.01\,E[E_0])^2$ and $Var(\dot{E}) = (0.01\,E[\dot{E}])^2$, so that the initial strain measure has extremely large expected value and it still stochastically increases; the time scale for all those experiments marked on the horizontal axis is given of course in years. A general observation is that all of those characteristics decrease together with a time increment, not only the expected value. The elastomer shear modulus become closer to the matrix rather together with the time being and the random distribution of the output coefficient *f* converges with time to the Gaussian one, however the coefficient of variation also tends to 0 (for at least 60% silica). The interrelations between different elastomers are the same for expectations, asymmetry and kurtosis – larger values are obtained for silica than for the carbon black and the higher volumetric ratio (in percents) the higher values of those probabilistic characteristics; this result remains in the perfect agreement with Figs. 22-25 (showing an initial state to this analysis).

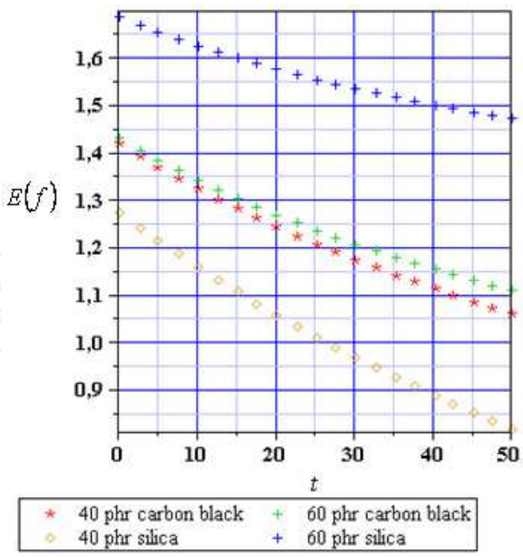


Fig. 26. The expected values for the power-law cluster breakdown to the scalar variable E

The coefficient of variation exhibit exactly the inverse interrelations – higher values are typical for silica reinforcement and for smaller amount of the reinforcing particles in the

elastomer specimen. For 40% silica the expected value of the reinforcement coefficient f becomes smaller than 1 after almost 25 years of such a stochastic ageing. It is apparent that we can determine here the critical age of the elastomer when it becomes too weak for the specific engineering application or, alternatively, determine the specific set of the input data to assure its specific design durability.

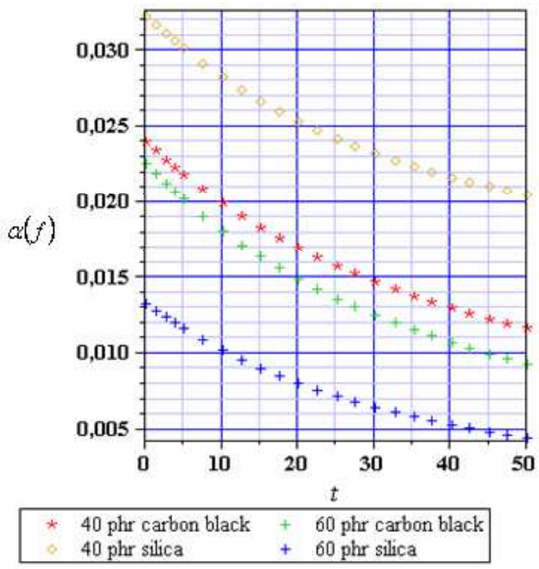


Fig. 27. Coefficients of variation for power-law cluster breakdown to the scalar variable E

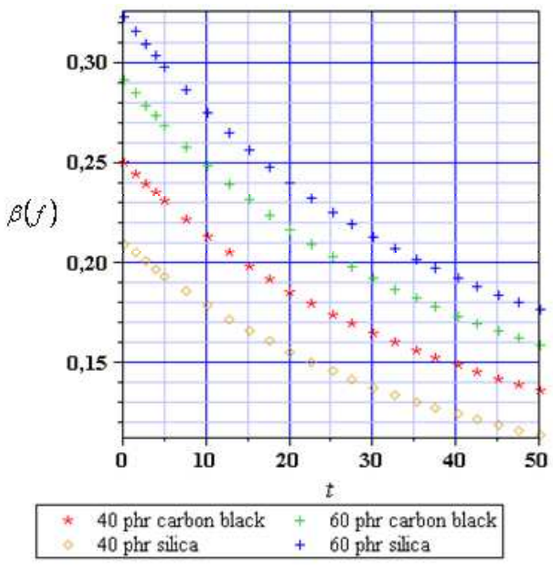


Fig. 28. Asymmetry coefficient for the power-law cluster breakdown to the scalar variable E

The input data set for the stochastic ageing of the elastomer according to the exponential cluster breakdown model is exactly the same as in the power-law approach given above. It results in the expectations (Fig. 30), coefficients of variation (Fig. 31), asymmetry coefficients

(Fig. 32) and kurtosis (Fig. 33) time variations for $t \in [0, 50\ years]$ . Their time fluctuations are generally similar qualitatively as before because all of those characteristics decrease in time. The expectations are slightly larger than before and never crosses a limit value of 1, whereas the coefficients are of about three order smaller than those in Fig. 27. The coefficients $\beta(t)$ are now around two times larger than in the case of the power-law cluster breakdown. The interrelations between the particular elastomers are different than those before – although silica dominates and $E[f]$ increases together with the reversed dependence on the reinforcement ratio, the quantitative differences between those elastomers are not similar at all to Figs. 26-27.

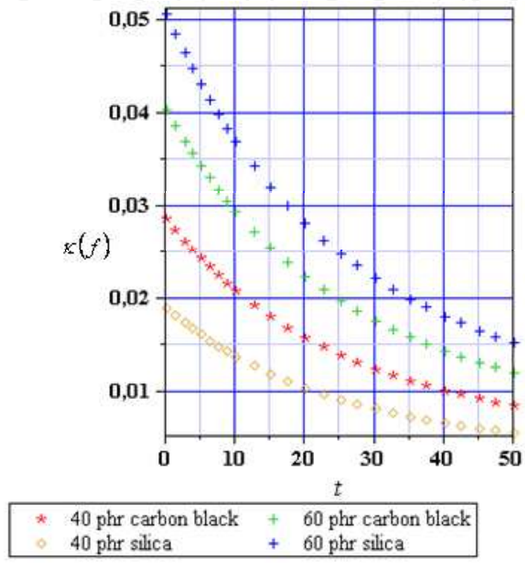


Fig. 29. The kurtosis for the power-law cluster breakdown to the scalar variable E

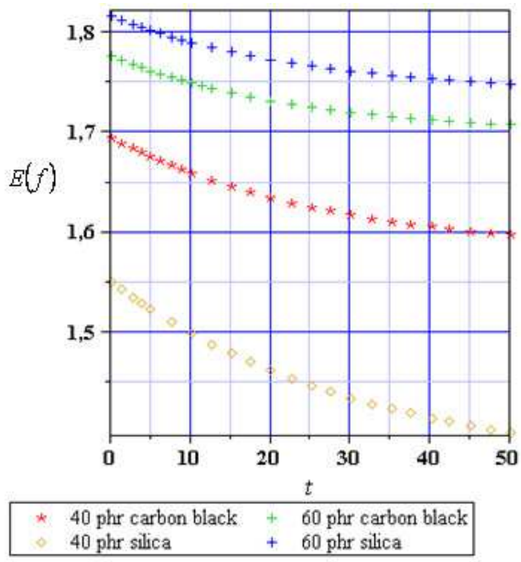


Fig. 30. The expected values for the exponential cluster breakdown to the scalar variable E

The particular elastomers coefficients of asymmetry and kurtosis histories show that larger values are noticed for the carbon black than for the silica and, at the same time, for larger volume fractions of the reinforcements into the elastomer.

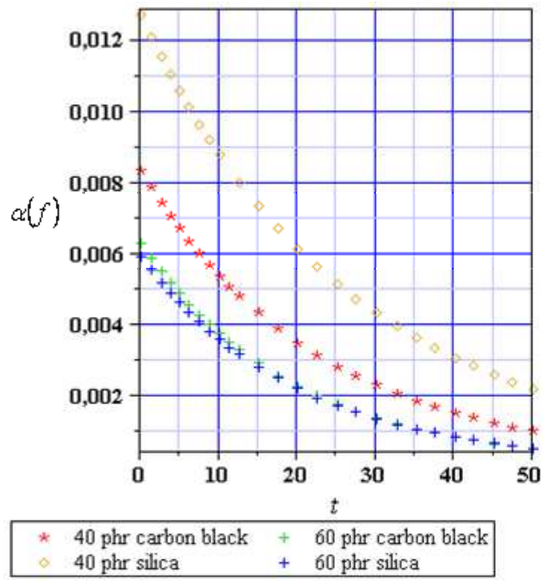


Fig. 31. Coefficients of variation for exponential cluster breakdown to the scalar variable E

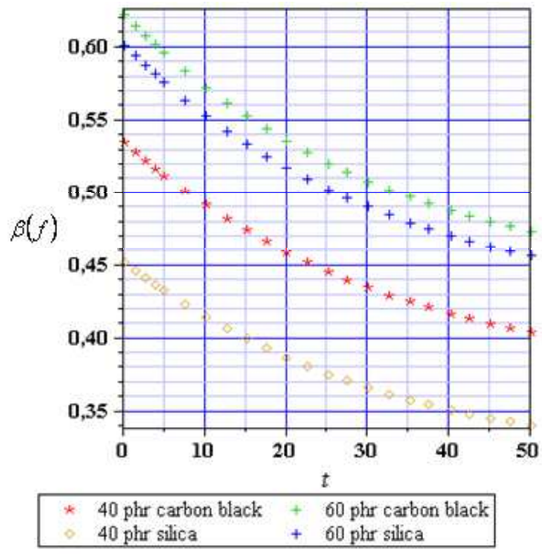


Fig. 32. Asymmetry coefficient for the exponential cluster breakdown to the scalar variable E

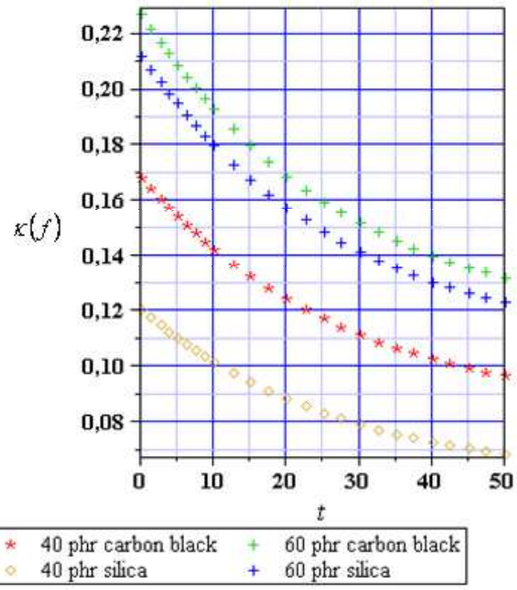


Fig. 33. The kurtosis for the exponential cluster breakdown to the scalar variable E

## 6. Concluding remarks

1. The computational methodology presented and applied here allows a comparison of various homogenization methods for elastomers reinforced with nanoparticles in terms of parameter variability, sensitivity gradients as well as the resulting probabilistic moments. The most interesting result is the overall decrease of the probabilistic moments for the process $f(\omega;t)$ together with time during stochastic ageing of the elastomer specimen defined as the stochastic increase of the general strain measure $E$. For further applications an application of the non-Gaussian variables (and processes) is also possible with this model.
2. The results of probabilistic modeling and stochastic analysis are very useful in stochastic reliability analysis of tires, where homogenization methods presented above significantly simplify the computational Finite Element Method model. On the other hand, one may use the stochastic perturbation technique applied here together with the LEFM or EPFM approaches to provide a comparison with the statistical results obtained during the basic impact tests (to predict numerically expected value of the tensile stress at the break) (Reincke et al., 2004).
3. Similarly to other existing and verified homogenization theories, one may use here the energetic approach, where the effective coefficients are found by the equity of strain energies accumulated into the real and the homogenized specimens and calculated from the additional Finite Element Method experiments, similarly to those presented by Fukahori, 2004 and Gehant et al., 2003. This technique, nevertheless giving the relatively precise approximations (contrary to some upper and lower bounds based approaches), needs primary Representative Volume Element consisting of some reinforcing cluster.

## 7. Acknowledgment

The first author would like to acknowledge the invitation from Leibniz Institute of Polymer Research Dresden in Germany as the visiting professor in August of 2009, where this research has been conducted and the research grant from the Polish Ministry of Science and Higher Education NN 519 386 686.

## 8. References

Bhowmick, A.K., ed. (2008). *Current Topics in Elastomers Research*, CRC Press, ISBN 13: 9780849373176, Boca Raton, Florida

Christensen, R.M. (1979). *Mechanics of Composite Materials*, ISBN 10:0471051675, Wiley

Dorfmann, A. & Ogden, R.W. (2004). A constitutive model for the Mullins effect with permanent set in particle-reinforced rubber, *Int. J. Sol. Struct.*, vol. 41, 1855-1878, ISSN 0020-7683

Fu, S.Y., Lauke, B. & Mai, Y.W. (2009). *Science and Engineering of Short Fibre Reinforced Polymer Composites*, CRC Press, ISBN 9781439810996, Boca Raton, Florida

Fukahori, Y. (2004). The mechanics and mechanism of the carbon black reinforcement of elastomers, *Rubber Chem. Techn.*, Vol. 76, 548-565, ISSN 0035-9475

Gehant, S., Fond, Ch. & Schirrer, R. (2003). Criteria for cavitation of rubber particles: Influence of plastic yielding in the matrix, *Int. J. Fract.*, Vol. 122, 161-175, ISSN 0376-9429

Heinrich, G., Klűppel, M. & Vilgis, T.A. (2002). Reinforcement of elastomers, *Current Opinion in Solid State Mat. Sci.*, Vol. 6, 195-203, ISSN 1359-0286

Heinrich, G., Struve, J. & Gerber, G. (2002). Mesoscopic simulation of dynamic crack propagation in rubber materials, *Polymer*, Vol. 43, 395-401, ISSN 0032-3861

Kamiński, M. (2005). *Computational Mechanics of Composite Materials*, ISBN 1852334274, Springer-Verlag, London-New York

Kamiński, M. (2009). Sensitivity and randomness in homogenization of periodic fiber-reinforced composites via the response function method, *Int. J. Sol. Struct.*, Vol. 46, 923-937, ISSN 0020-7683

Mark, J.E. (2007). *Physical Properties of Polymers Handbook*, 2nd edition, ISBN 13: 9780387312354, Springer-Verlag, New York

Reincke, K., Grellmann, W. & Heinrich, G. (2004). Investigation of mechanical and fracture mechanical properties of elastomers filled with precipitated silica and nanofillers based upon layered silicates, *Rubber Chem. Techn.*, Vol. 77, 662-677, ISSN 0035-9475


**Stochastic Control**

Edited by Chris Myers

ISBN 978-953-307-121-3

Hard cover, 650 pages

**Publisher** Sciyo

**Published online** 17, August, 2010

**Published in print edition** August, 2010

Uncertainty presents significant challenges in the reasoning about and controlling of complex dynamical systems. To address this challenge, numerous researchers are developing improved methods for stochastic analysis. This book presents a diverse collection of some of the latest research in this important area. In particular, this book gives an overview of some of the theoretical methods and tools for stochastic analysis, and it presents the applications of these methods to problems in systems theory, science, and economics.



**InTech Europe**

University Campus STeP Ri
Slavka Krautzeka 83/A
51000 Rijeka, Croatia
Phone: +385 (51) 770 447
Fax: +385 (51) 686 166
www.intechopen.com

**InTech China**

Unit 405, Office Block, Hotel Equatorial Shanghai
No.65, Yan An Road (West), Shanghai, 200040, China
中国上海市延安西路65号上海国际贵都大饭店办公楼405单元
Phone: +86-21-62489820
Fax: +86-21-62489821

IntechOpen